Sensors and Materials, Vol. 18, No. 1 (2004) 035–048
MYU Tokyo

S & M 0628

Design and Fabrication of Heated Microchannels

Minhee Kim, Roman Brukh, Sumit Kishore,
Somenath Mitra* and Durgamadhab Misra[1]

Department of Chemistry and Environmental Science, New Jersey Institute of Technology,
University Heights, Newark, NJ 07103, USA
[1]Department of Electrical and Computer Engineering, New Jersey Institute of Technology,
University Heights, Newark, NJ 07103, USA

(Received May 19, 2005: accepted October 14, 2005)

Key words: microheater, microfluidics, MEMS, micromachining

The development of lab-on-a-chip and miniature sensors often involves microheaters to carry out reactions and sample preparation on the microscale level. In this paper, we present the design and fabrication of heated microchannels by sputtering a metal film to form a resistive heater. The devices were fabricated on a 6-inch silicon substrate via conventional oxidation, photolithography, chemical wet etching, and metal deposition steps. A surface temperature as high as 360ºC could be attained using an aluminum alloy as the conducting layer. The response time of the heater was short and maximum temperature could be attained within 10–30 s. The heater showed excellent long-term stability under repeated temperature cyclings. A heat transfer model that fits the experimental data quite well is presented. The model can be used to design heated microchannels of desired dimensions.

1. Introduction

Microfluidic devices are being used in various applications, such as chemical analysis, reaction engineering, drug discovery, electronics chip cooling, flow sensors and biomedical devices.[1] Microfluidics are also being employed in separation techniques, such as gas chromatography,[2–4] liquid chromatography[5] and electrophoresis.[6-8] It has been demonstrated that it is possible to put a conventional chemical laboratory onto a single microchip to carry out a large number of parallel analyses.[9] Performance enhancement, high throughput, low power consumption, reduction in the sample size, and low cost are some of the advantages of such miniaturized devices. Moreover, the combination of chemical analysis and traditional electronics on a single silicon chip can lead to rapid and inexpensive manufacturing processes.[10] Noteworthy among the different applications is microfabricated capillary electrophoresis for DNA sequencing.

*Corresponding author, e-mail address: mitra@njit.edu

Many microfluidic devices require technologies for temperature control because reactions and sample preparations need to be carried out at higher temperatures. It is often important to heat a particular area of a working element while the rest of the system is maintained at a lower temperature.[11] The need for local microheating and maintaining a constant temperature necessitates the development and fabrication of efficient microscaled heaters. For example, the polymerase chain reaction (PCR) for DNA amplification requires fast temperature cycling.[12] Temperature manipulation is also important in chromatography (especially gas chromatography) and sorbent sampling applications.[13]

The development of several microfabricated heating devices has been reported.[14–20] Microheating elements have been made either by the deposition of polysilicon layers[21] or by heavy doping of silicon substrates.[16] Many of the current microheaters use fabrication techniques in which a selective etch of the bulk silicon followed by implanting high concentrations of dopants (the typical range of the ion dose is between 10^{19} to 10^{21} atoms/cm^3) to achieve a higher level of electrical conductivity in the heater region.[17] Studies of micromachined heaters for thermomechanical data storage have been conducted.[22] Single-crystal silicon cantilevers with integrated resistive heaters have also been demonstrated.[22] These cantilevers were made electrically conductive by implanting heavy ions. The heater region was doped with phosphorous at 1.5×10^{21} atoms/cm^3 and the legs at 10^{20} atoms/cm^3. Ion implantation over a device allows the option of further anisotropical etching of the underlying substrate while providing localized heating. However, heavy-ion implantation is an expensive process.[18,23]

Silicon-on-insulator (SOI) technology is another way to fabricate microheaters and is known to be simpler than either the deposition of polysilicon layers or the heavy doping of silicon. A thermally isolated microheater suspended 2 μm above a wafer substrate has been fabricated using SOI wafer with a 2 μm buried oxide layer on the silicon substrate.[18] This method is simpler than the other methods because it involves only one masking step. However, it also requires heavy boron or phosphorous doping to form the conductive layer (approximately > 10^{19} atoms/cm^3). Experimental results obtained using these devices have shown that temperatures in excess of 1000°C can be achieved at low power.[23] The heaters can be as small as 500 μm^2. It has also been demonstrated that these heaters reduce contact resistance so that there is less unwanted heating at the contacts. However, once the maximum temperature is reached, any further increase in current only broadens the active area of the heating element. Thus, continued operation in this region leads to device weakening and eventually device burn out.

In this study, we employed a simple and inexpensive process for the fabrication of microheaters for microfluidic applications (particularly heated microchannels) using standard photolithographic techniques and chemical wet etching. This study is focused on the fabrication and testing of metal-deposited heaters. Their temperature characteristics have been studied under various conditions. The heaters were also coated with spin-on-glass (SOG) to see how this coating changes the heating characteristics. The stability of the heater under repeated pulses was also studied to simulate real-world applications. A comparison is also made with heaters of similar dimension formed by boron implantation in silicon.

2. Experimental Methods

The microheaters used in MEMS could be fabricated on quartz or borosilicate glass wafers, two common materials for photolithographic fabrication. Quartz works well in electrophoresis because it is not only a good electrical insulator, but it is also transparent to UV required for absorbance and fluorescence detection. Quartz substrates also generate high electro-osmotic flow rates and have favorable surface characteristics after fabrication by etching. Silicon is also popular in microfluidic applications because it is possible to embed both fluid control and fluid detection by integrated circuits on one substrate. Typical fluidic devices such as microreactors and microfluidic capillaries are 2–3 cm^2 in size and are made of silicon, glass, quartz or plastic that is either etched or molded. The etched channels and chambers are usually covered with Pyrex, glass or silicon to contain the sample and reagent.

The materials used for this microheater were <100> oriented, 6-inch, p-type (boron doped), single-side polished silicon wafers, with a thickness of 575 μm and a resistivity range of 10–25 Ω-cm. The chip layout was fabricated on a Sun Sparc workstation using an IC tool in Mentor Graphics (Wilsonville, OR). All fabrications except ion implantation were carried out at the New Jersey Institute of Technology Microelectronics Research Center clean room. Ion implantation was carried out at Ion Implant Services (Sunnyvale, CA). The implantation processes were simulated using Stanford University process emulator (SUPREM III) simulation package.

Figure 1 shows the step-by-step processing of the wafer and the cross-sectional view after each step. The first step was steam oxidation of the wafers to grow the oxide layer. This was followed by low-pressure chemical vapor deposition (LPCVD) to deposit the silicon nitride layer (Si_3N_4). Then, the wafers with 2000-Å-thick oxide and 1550-Å-thick nitride were patterned using standard UV lithography. The patterned wafers were etched using reactive ion etching (RIE). RIE is a combination of many sequential plasma etching steps and has the major advantage of etching silicon dioxide over the silicon layers. After this, anisotropic etching with potassium hydroxide (KOH, 45% by volume) was performed at 95ºC for 3.5 h at an etch rate of 1.66 mm/min. The etch rate depends on the doping and crystal orientation of silicon, and the type/temperature of the KOH solution used. It was typically on the order of about a micron per minute.

Two different approaches were taken to form the conducting layer in the microheater. The first was the deposition of a metal in the channel by sputtering, and the second was doping with boron via ion implantation. The metal source used in this study was an aluminum alloy which was 99% aluminum, the rest being silicon and copper. The reason for using the silicon-aluminum alloys was to prevent silicon from reacting with the deposited aluminum, which could cause spiking or short circuits.[24] A set of etched wafers were sent to an ion implantation service. In ion implantation, dopant atoms are ionized, formed into a beam, and swept across the wafer. The bombarding atoms enter the substrate and come to rest below the surface. The dopant used in this study was boron.

Once all process steps were completed, each micro-fabricated heater was tested individually. The heater was mounted under a four-point probe station (Cascade Microtech Inc., Beaverton, OR). Different voltages were applied to each device to test the heating

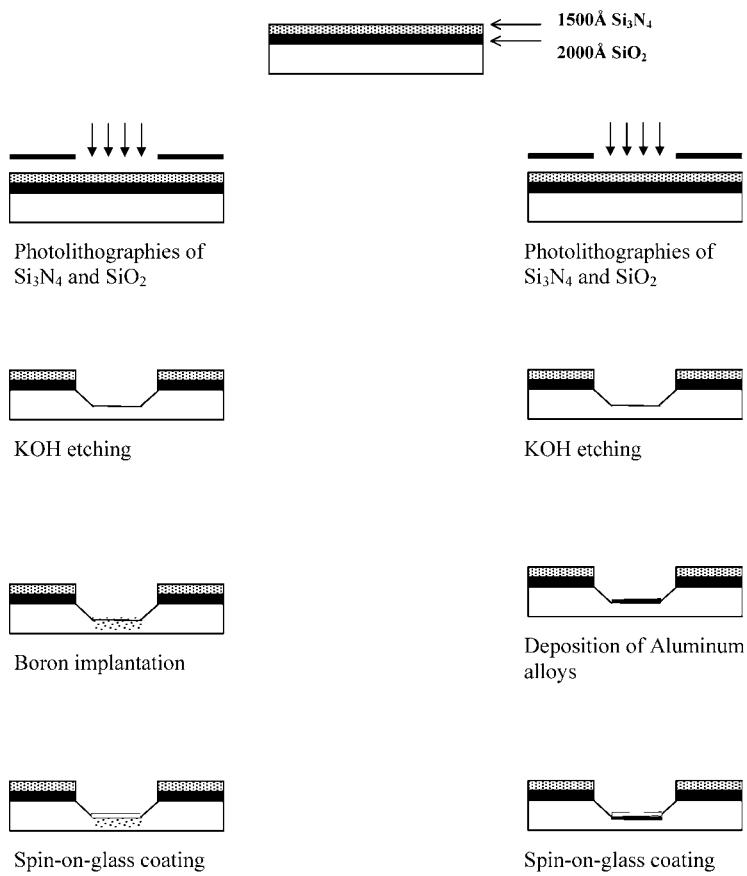

Fig. 1. Steps in fabrication of microheater.

characteristics as a function of time. The voltage was applied through tungsten probes with 0.5 mm tips. The Tegam 871 digital thermometer, in conjunction with a Kapton p08508-86 K thermocouple probe was placed on a contact pad to measure the channel temperature.

3. Result and Discussion

Etching the <100> oriented silicon wafers in KOH (45% by volume) produced wells with 54° angle sidewalls. Since the substrate was <100> oriented, chemical wet etching produced the channels anisotropically with low aspect ratios. As a result, the channel geometry was trapezoidal as shown in Fig. 2(a). Several channel configurations were fabricated with widths between 50 and 456 μm, depths between 35 and 350 μm, and lengths between 6 and 19 cm. The separation distance between the channels was varied such that the entire microheater fits in an 1 cm^2 area. Figure 2(b) shows a fabricated heater with two contact pads.

The resistance R of the circuit element can be calculated as

$$R=\gamma L/tb, \tag{1}$$

where γ is the resistivity of the conducting material,[25] t is the thickness of the conducting material, L is the overall length of the channel, and b is the width of the channel.

The different channel configurations shown in Table 1 were fabricated on a single wafer to study the heating characteristics. The heater was formed by depositing 1 μm of conducting film on the channels.

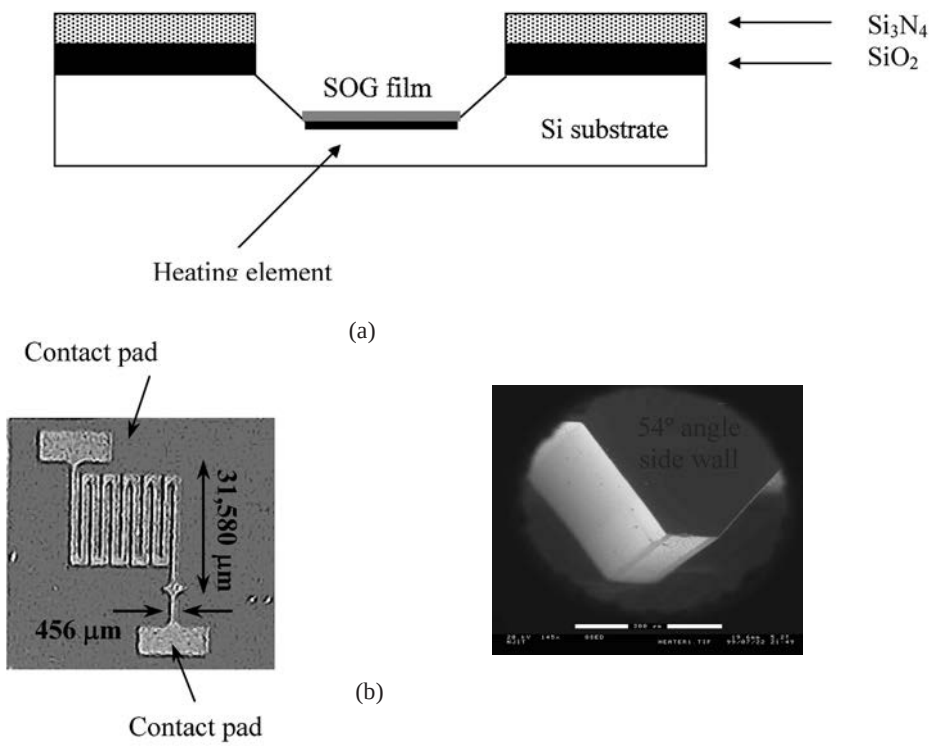

Fig. 2. (a) Cross section of etched channel of microheater. (b) Photograph and SEM image of heated channel on silicon wafer.

The heating characteristics of the microheater at different voltages as a function of time were studied. The heater was placed on a table, opened to air and connected to tungsten probes. The initial temperature was between 23 and 25ºC for all the heaters. The temperature profiles of heater A with 15, 30, and 36 V across it are shown in Fig. 3. It took an average of 10–20 s to reach the maximum temperature. The time needed to cool the microheater to its initial temperature was about 5 s. The microheaters cooled faster than they heated up. All heat was lost to surrounding air and through the silicon body of the heater. In all cases, temperature stabilized in less than 30 s. Table 1 shows the maximum temperatures attained for different heater designs. As shown in Fig. 3 and in Table 1, a temperature in excess of 350ºC could be achieved with approximately 36 V. It should be noted that higher temperature could be reached by applying higher voltage or changing film thickness.

Table 1
Resistances of thin-film microheaters of different dimensions and maximum temperature reached at 40 V.

Heater Type	*b* μm	*L* cm	Resistance of metal film, Ohm	Max. temperature, °C
A	456	6.7	5.8	387
B	300	6.0	14.2	247
C	456	18.7	21.0	137
D	50	6.0	40.0	86

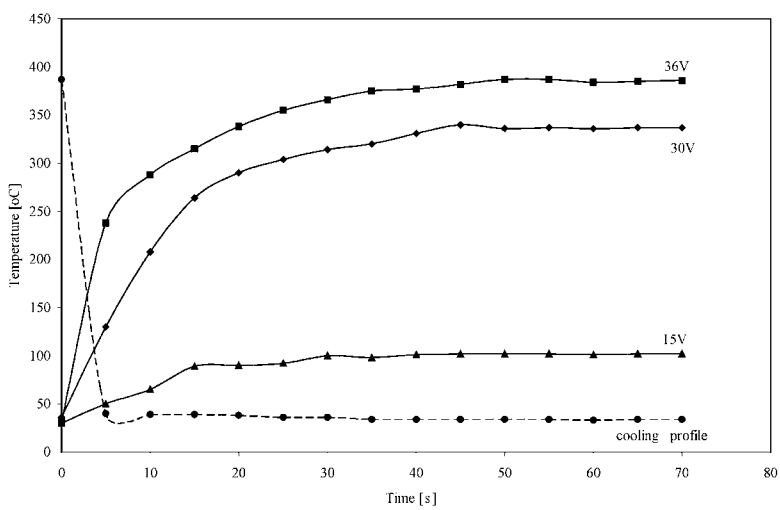

Fig. 3. Temperature profile of heater type A with 1 μm metal film when different voltages were applied.

3.1 *Comparison with heater made by boron implantation*

The second set of heaters was made by low-dose boron implantation. Resistance was a function of dopant concentration. The wafers were annealed at 400°C in the presence of argon. The annealing brought some of the dispersed dopant ions closer to the surface, thus forming a uniform conductive layer. Inadequate annealing could result in the bulk of the implanted ions being distributed too deeply into the substrate to contribute to conductivity. Two different implantation regimes were tried. In addition, in an effort to improve heating characteristics, each was subjected to two different annealing times.

As preliminary estimations of energy and dose from the boron source, the concentration following annealing was simulated using a computer program called SUPREME III (Stanford University process emulator). This determined the penetration depth of the boron atoms. For the first run, the implantation energy was 80 keV at a dose of 1×10^{14} atoms/cm^3. For the second run, implantation was carried out at a higher dose of 2×10^{15} atoms/cm^3 at 100 keV. After annealing (dopant activation), boron ions rest at various depths in the wafer. They are centered at a depth called the projected range at which the diffusion depth can be predicted.

The sheet resistances with boron doping were much higher than those obtained by metal deposition. They are listed in Table 2. For the first implant (80 keV, 1×10^{14}/cm^2, 40 min annealing at 900°C), the concentration was 5×10^{19}/cm^3 at a depth of 0.4 μm with a γ of 1.8×10^{-3} Ω-cm. For the second implant (100 keV, 2×10^{15}/cm^2, 20 min anneal at 1050ºC), the concentration was 1×10^{20}/cm^3 at a depth of 1 mm with a γ of 5×10^{-4} Ω-cm. The second scheme brought about an order of magnitude decrease in the resistance of the channels. However, even this resistance was quite high, suggesting that even a higher dose of doping was necessary, probably in the range of 10×10^{19}/cm^3 to 10^{21}/cm^2. However, such heavy doping would increase the fabrication costs significantly.

Table 3 shows the maximum temperature attained by different fabricated heaters under different annealing conditions. It shows that annealing beyond 20 min did not increase the maximum temperature attainable by the heaters. For example, channel type A with a metal heater could attain a temperature up to 387ºC (Table 1), while the maximum temperature attained with boron doping was 64.3ºC. The heating profile of the doped wafer was similar to the heaters with metallic layers. Conductivity depended on the dopant concentration.

3.2 *Effect of glass coating*

It is expected that for many applications, the heater would be coated with glass, polymer or silicon. For example, those used in electrophoresis and chromatography

Table 2
Resistance of boron implanted heating layer.

Heater type	R(kΩ)-implant at 80 keV, 1×10^{14} cm^2, 900ºC	R(Ω)-implant at 100 keV, 2×10^{15} cm^2, 1050ºC
A	0.54	66.7
B	1.95	125
C	25.5	1600
D	∞	73

Table 3
Maximum temperature measured (°C) for boron-implanted heaters at 40 V.

Heater type	Boron Implanted, annealed			
	80 keV 1×10^{14} cm^2 400 min annealing	80 keV 1×10^{14} cm^2 60 min annealing	100 keV 2×10^{15} cm^2 20 min annealing	100 keV 2×10^{15} cm^2 40 min annealing
Diffusion Depth	0.3 μm	0.4 μm	1 μm	1.2 μm
A	32.8	36.6	64.3	62.0
B	25	26.1	44.0	38.1
C	26.7	26.7	26.0	27.3
D	25	25.9	40.3	40.4

require glass-based surfaces because of the ease of chemical modification using organosilanes.[26] Since organic polymers have low adhesivity for silicon or metal, a layer of glass can be used on the substrate for modification. Hence, a coat of spin-on-glass (SOG) was applied on the channels to see how it affected the temperature characteristics. The thickness was controlled by the speed of the spinner. For the "6" wafers, 4 ml of SOG was applied at 2000 RPM for 2 s. This achieved a glass thickness of 1 mm. This was followed by hard plate baking at 80, 150 and 250ºC for 40 s each. Then, the wafers were cured in a furnace at 425°C for 60 min.

The increase in temperature as a function of time with the spin-on-glass coating is presented in Fig. 4 at an applied voltage of 43 V. In all cases, the temperature stabilized in less than 10 s. The glass coating imposed a higher resistance to heat transfer. The maximum temperature attained on the spin-on-glass-coated surface was significantly lower. At an applied voltage of 36, temperatures were close to 390°C in the absence of the glass coating, whereas the maximum temperature with spin-on-glass was 120°C at an applied voltage of 43. Thinner glass layers are desired to attain higher temperatures.

3.3 *Stability of heater under repeated cycles*

The stability of the heater to alternate heating and cooling was studied by applying a series of repeated voltage pulses. A sequence of 2 s and 30 V pulses were applied to heater A and the current was measured. This was repeated every two min for 5 h. The results are shown in Fig. 5. The heater could reach a constant current of 1.6 A for each voltage pulse. The temperature was as high as 100ºC within 2 s. The resistance of the heater did not change during the 148 cycles performed. In another set of experiments, the heater was cycled for 17 h (overnight). The current remained the same even after 486 cycles. The relative standard deviation of the current over 148 cycles was 0.620%. This demonstrates the ruggedness of the microheater during the repeated cyclings. Measurements were made

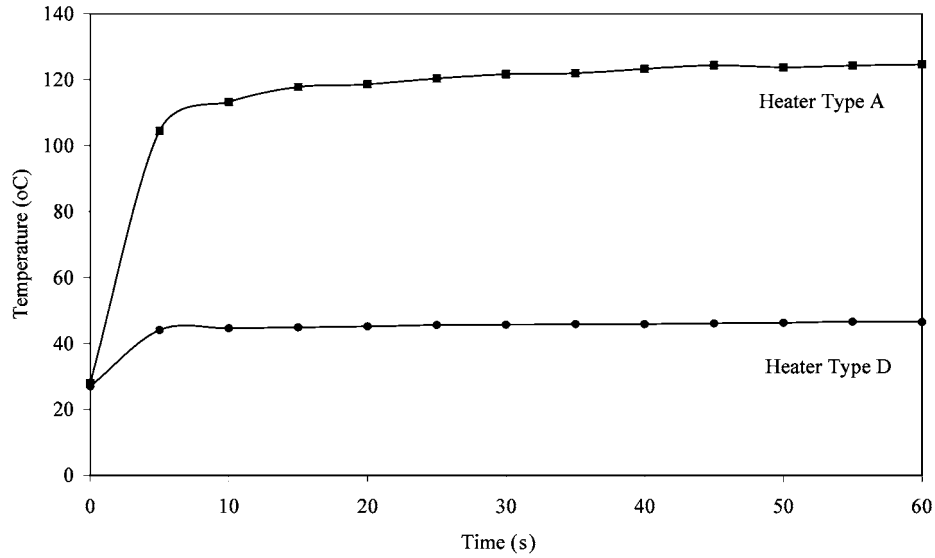

Fig. 4. Temperature characteristics of 1 mm metal-deposited heater types A and D with spin-on-glass.

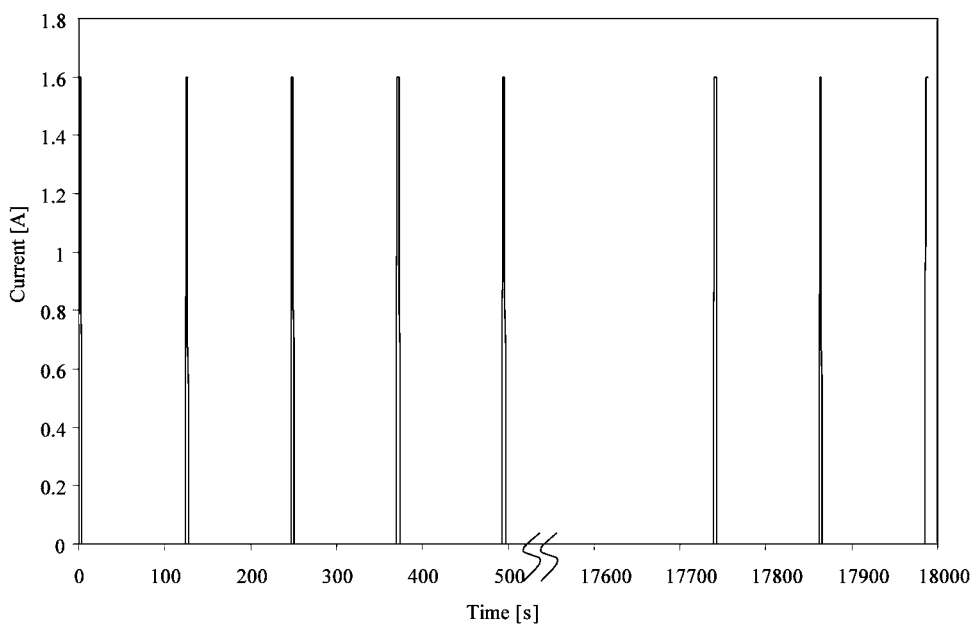

Fig. 5. Current profile for each voltage pulse to heater type A; 30 V pulses were applied every 2 min for 2 s.

for repeated cyclings over 17 h. However, the heater was used many times over months.

3.4 *Modeling and design of microheaters*

The temperature reached by the heater depends upon its dimensions according to eq. (1) and also on the voltage applied. To design heated microchannels, the heat transfer theory was used to develop a model for the microheater and to predict the temperature characteristics of heaters with different dimensions. Heat generated by the electric current in a thin-film heater [27] is given by

$$q_G = I^2 \gamma L, \tag{2}$$

where I is the electric current.

The heat generated is lost through the heater body to the surroundings by conduction (q_c), radiation (q_r) and convection (q_f) given by

$$q_{lost} = q_c + q_r + q_f, \tag{3}$$

where

$$q_c = (k/s)(T_h - T_{b\infty}) \tag{4}$$

$$q_r = \sigma \varepsilon b L (T_h^4 - T_\infty^4) \tag{5}$$

$$q_f = hbL(T_h - T_\infty). \tag{6}$$

Here, k and s are the thermal conductivity and thickness of the silicon substrate, respectively, ε and σ are the emittance and the Stefan-Boltzmann constant, respectively, h is the convective heat transfer coefficient for heat transferred to a fluid, and T_h , $T_{b\infty}$ and T_∞ are the temperatures of the heated film, heater body, and the surrounding air, respectively. Since the heated channels are small compared with the substrate bulk, the temperature rise of the heater body was not significant, and its temperature is approximately equal to the temperature of the surroundings, i.e., $T_{b\infty} \approx T_\infty$.

Equation (5) can be linearized by factoring the term $T_h^4 - T_\infty^4$ to obtain a solution expressed as[27]

$$q_r = \sigma \varepsilon b L (T_h^4 - T_\infty^4) = \sigma \varepsilon b L (T_h^2 + T_\infty^2)(T_h + T_\infty)(T_h - T_\infty). \tag{7}$$

By solving this equation numerically within the practical temperature range (up to 450ºC), it was found that eq. (7) could be reduced to

$$q_r \approx \sigma \varepsilon b L (4.3 T_m^3)(T_h - T_\infty). \tag{8}$$

The largest error in this approximation was computed to be no more than ±6%. Substituting eqs. (4), (5) and (6) into eq. (3),

$$q_{lost} = (k/s)(T_h - T_{b\infty}) + \sigma \varepsilon b L (4.3 T_m^3)(T_h - T_\infty) + hbL(T_h - T_\infty) \tag{9}$$

$$q_{\text{lost}} = \{k/s+\sigma\varepsilon bL(4.3T_m^3) + hbL\}(T_h–T_\infty) \quad (10)$$

or

$$q_{\text{lost}} = U_T bL(T_h–T_\infty), \quad (11)$$

where

$$U_T = k/sbL + se(4.3T_m^3) + h. \quad (12)$$

Here, U_T is the total heat transfer coefficient that reflects the overall heat loss to the surroundings by conduction, radiation and convection. The calculations showed that the values of radiative heat transfer coefficient $\sigma\varepsilon bL$ $(4.3T_m^3)$ contributed only 0.0003% to the value of U_T, and for all practical purposes it can be ignored. Thus, heat was mainly lost by conduction and convection.

Substituting eqs. (2) and (11) into eq. (3),

$$I^2\gamma L = U_T bL(T_h–T_\infty) \quad (13)$$

and considering Ohm's law $I = V/R$ and eq. (1), eq. (13) can be written in terms of applied voltage as

$$V^2b^2t^2/\gamma L = U_T bL(T_h – T_\infty). \quad (14)$$

From this equation, the temperature of the heated film T_h can be calculated as

$$T_h = V^2bt^2/\gamma U_T L^2 + T_\infty. \quad (15)$$

Equation (15) was used to calculate the temperature of the film as a function of applied voltage. The experimental values of the heater temperature were well represented by this model. The results for heater A are shown in Fig. 6. The calculated values of the total heat transfer coefficient U_T and experimental temperatures for the different types of heaters A, B, C, and D ranged from 6×10^6 to 1×10^5 W/m^{2}K. These were well within the range of variability commonly encountered in heat transfer calculations.[28–30] This demonstrated that the model represented the microheater quite well.

The value of the total heat transfer coefficient U_T depends upon temperature, fluid properties, flow conditions, and channel geometry. In addition, the dimensions and the uniformity of the deposited heating film sometimes can be difficult to control. Therefore, some deviations of experimental data from the predicted values are to be expected. Moreover, it is well known that the heat transfer coefficients can vary over a relatively large range.[30] Equation (15) was used to simulate microheater film temperature as a function of film dimensions. The same material was used for heating films. However, these calculations can be performed for any other material of known resistivity. The model predicts the temperature of the heated film. The temperature of a particular fluid (gas or liquid) can be calculated on the basis of heater temperature and the thermal properties of the fluid, and flow conditions. The calculated film temperatures are shown in Figs. 7, 8, and 9, which can be used for estimating the heater parameters. As shown in Fig. 7, the

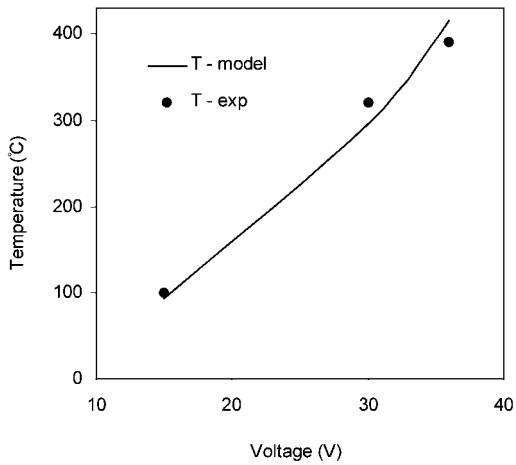

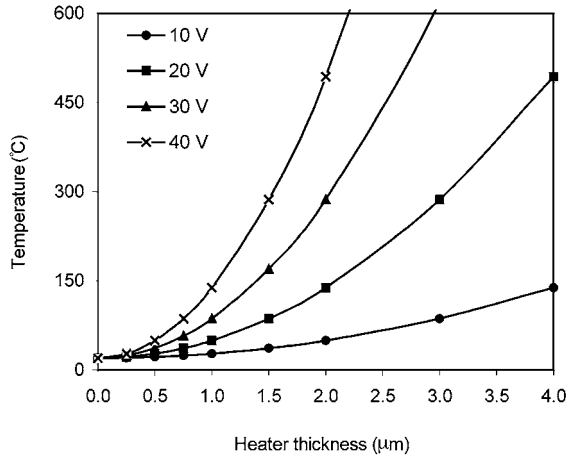

Fig. 6 (left). Comparison of experimental and predicted temperatures of heater A.
Fig. 7 (right). Calculated temperature as function of aluminum alloy film thickness (film width, 250 mm; length, 10 cm).

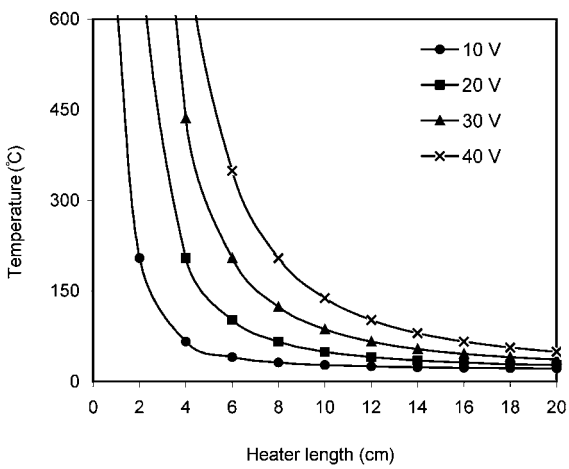

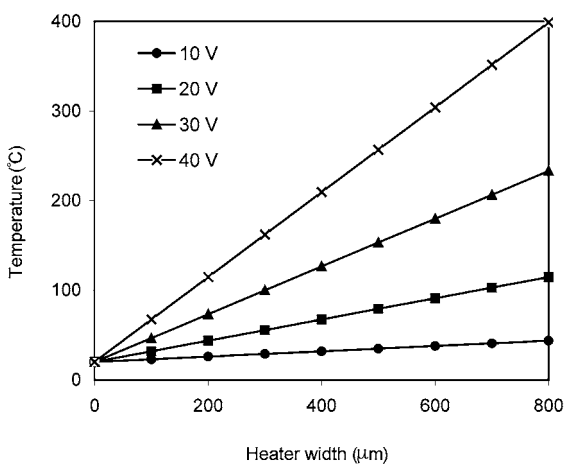

Fig. 8 (left). Calculated temperature as function of aluminum alloy film length (film width, 250 mm; thickness, 1 mm).
Fig. 9 (right). Calculated temperature as function of aluminum alloy film width (film thickness, 1 mm; length, 10 cm).

increase in film thickness had a large effect on heater temperature due to the rapid decrease in heater resistance. An increase in heater length increased heater resistance and subsequently decreased heater temperature. This is shown in Fig. 8. While film width also affected temperature, its effects were not as pronounced as those of thickness or length. Temperature increased linearly with width as predicted by eq. (15) and as shown in Fig. 9. Temperature increased exponentially with film thickness and linearly with film width. The higher the applied voltage, the greater was the increase in temperature. The effect of film length on temperature was more significant in short-film heaters (less than 8–10 cm). At lower voltages, the change in temperature appeared to be more significant.

4. Conclusions

Microfabricated heaters with sputtered metal layers were fabricated. Rapid heating to temperatures as high as 360ºC was possible. Repeated heatings did not lead to device weakening or burning out. A comparison with low-dose boron implantation showed that the metal-deposited heaters were able to reach higher temperatures under the same conditions. The application of spin-on-glass on the heater surface reduced the maximum attainable temperature, but temperatures as high as 100ºC were still possible. On the whole, metal deposition is a relatively simple method to fabricate heaters for lab-on-a-chip applications. A developed heat transfer-based model can be used to predict a temparature-voltage ralationship quite well and can be used to design heaters of different dimensions.

Acknowledgement

This project was supported in part by grants from the USEPA Center for Airborne Organics at MIT and the New Jersey Commission on Science and Technology through the New Jersey MEMS initiative. We are grateful to Dr. Dentcho Ivanov, Dr. Kenneth Farmer, Dr. Rajendra Jarwal and Kenneth O'Brien for their support.

References

1 G. J. M. Bruin: Electrophoresis (2000) 3931.
2 S. C. Terry, J. H. Jerman and J. B. Angell: IEEE Trans. Electron Devl. **ED-26** (1979) 1880.
3 R. R. Reston and E. S. Kolesar: Journal of Microelectromechanical Systems **3** (1994) 134.
4 M. L. Hudson, R. Kottenstette, C. M. Matzke, G. C. F.-Mason, K. A. Shollenberger, D. R. Adkins and C. C. Wong: Micro-Electro-Mechanical Systems, ASME **66** (1998) 207.
5 A. Manz, Y. Miyahara, J. Miura, Y. Watanabe, H. Miyaqi and K. Sato: Sens. Actuators, B **1**: (1990) 249.
6 D. J. Harrison, P. G. Glavina and A. Manz: Sens. Actuators, B **10** (1993) 107.
7 D. J. Harrison, A. Manz, Z. Fan, H. Ludi, and H.M. Widmer: Analytical Chemistry **64** (1992) 1926.
8 S. C. Jacobson, R. Hergenroder, L. B. Koutny, R. J. Warmack and J. M. Ramsey: Analytical Chemistry **66** (1994) 1107.
9 M. Freemantle: Downsizing Chemistry (C&EN, Washington D.C, 1999) p.27.

10 R. K. Lowry: Analytical Chemistry **58** (1986) 23.
11 E. T. Lagally, P. C. Simpson and R. A. Mathies: Sens. Actuators, B **63** (2000) 138.
12 A. T. Woolley, D. Hadley, P. Landre, A. J. deMello, R. A. Mathies and M. A. Northrup: Analytical Chemistry **68** (1996) 4081.
13 K. A. Rubinson and J. F. Rubinson: Contemporary instrumental analysis (Prentice-Hall, 2000) p. 577
14 M. Kim and S. Mitra: Journal of Chromatography A **996** (2003) 1.
15 S. Glod, D. Poulikakos, Z. Zhao and G. Yadigaroglu: International Journal of Heat and Mass Transfer **45** (2002) 367.
16 R. L. Bayt and K. S. Breuer: Sens. Actuators, A **91** (2001) 249.
17 S. Wolf and R. N. Tauber: Process Technology (Lattice Press, New York, 1986) p. 5.
18 C. A. Straede and N. J. Mikkelsen: Surface and Coatings Technology **103** (1998) 1991.
19 Z. Zhao, S. Glod and D. Poulikakos: International Journal of Heat and Mass Transfer **43** (2000) 281.
20 S. Moller, J. Lin and E. Obermeir: Sens and Actuators, B **25** (1995) 343.
21 S. Mitra, C. Feng, L. Zhang, W. Ho and G. McAllister: J. Mass Spectrom. **34** (1999) 478.
22 H. J. Mamin and D. Rugar: Applied Physics Letters **61** (1992) 8.
23 M. Faghri and B. Sunden: Heat and Fluid Flow in Microscale and Nanoscale Structures (WIT Press, 2004).
24 P. Van Zant: Microchip Fabrication (McGraw-Hill, New York, 1996).
25 S. M. Sze: Physics of Semiconductor Devices (John Wiley and Sons, New York, 1991) p. 5.
26 K. G. Proctor, S. K. Ramirez, K. L. McWilliams, J. J. Kirkland: In Chemically Modified Surfaces: Recent Developments, J. J. Pesek, M. T. Matyska and R. R. Abuelafiya: The Royal Society of Chemistry (Cambridge, 1996) p. 45.
27 F. Kreith and M. Bohn: Principles of Heat Transfer (Harper & Row Publishers, New York, 1986).
28 A. F. Mills: Basic Heat and Mass Transfer (Richard D. Irwin, 1995) p. 22.
29 F. M. White: Heat and Mass Trasfer (Addison-Wesley Publishing, New York, 1991) p. 26.
30 F. Incropera and D. DeWitt: Fundamentals of Heat and Mass Transfer (John Willey and Sons, New York, 2001) p. 8.